EUROPEAN ORGANIZATION FOR NUCLEAR RESEARCH

CERN-PH-EP/2008-011
June 6, 2008

Study of Hadronic Event Shape in Flavour Tagged Events in e^+e^- Annihilation at $\langle\sqrt{s}\rangle = 197$ GeV

L3 Collaboration

Abstract

Results are presented from a study of the structure of hadronic events in high-energy e^+e^- interactions detected by the L3 detector at LEP. Various event shape distributions and their moments are measured at several energy points at and above the Z-boson mass. The event flavour is tagged by using the decay characteristics of b-hadrons. Measurements of distributions of event shape variables for all hadronic events, for light (u, d, s, c) and heavy (b) quark flavours are compared to several QCD models with improved leading log approximation: Jetset, Herwig and Ariadne. A good description of the data is provided by the models.

Introduction

Hadronic events produced in e^+e^- annihilation have been a powerful tool to test the predictions of Quantum Chromodynamics (QCD) [1]. Perturbative QCD successfully accounts for many aspects of the hadronic decays of the Z boson [2]. The primary quarks from Z-boson decays first radiate gluons, which in turn may split into quark or gluon pairs. The quarks and gluons then fragment into observable hadrons. Perturbative QCD itself does not describe the fragmentation process. Instead several phenomenological models have been developed to describe fragmentation. These models provide a way to correct for the effects of fragmentation in the experimental data, which can then be compared with the perturbative QCD calculations directly.

The event shape variables which characterize the global structure of hadronic events are among the simplest experimental measurements sensitive to the parameters of perturbative QCD and fragmentation models. This article reports on the measurement of event shapes for hadronic events collected at LEP by the L3 detector at e^+e^- centre-of-mass energies $\sqrt{s} \geq 189$ GeV. Similar analyses were reported by all LEP experiments [3, 4].

Heavy flavour production in e^+e^- annihilation can be studied by exploiting the characteristics of heavy flavour decays. In the present study, hadronic events are separated into heavy (b) and light (u, d, s, c) flavours, and event shape variables are separately measured for these final states. This allows to test the modeling of heavy flavour mas effects. Earlier and similar measurements, at lower centre-of-mass energies, are reported in references [3] and [5].

Global Event Shape Variables

Event shape variables, insensitive to soft and collinear radiation, are built from linear sums of measured particle momenta. They are sensitive to the amount of hard-gluon radiation. Six global event shape variables are measured here. These are: thrust, scaled heavy jet mass, total and wide jet broadening, the C-parameter and the jet resolution parameter. These event-shape variables are defined below.

Thrust

The global event-shape variable thrust, T, [6] is defined as

$$T = \frac{\sum |\vec{p}_i \cdot \vec{n}_\mathrm{T}|}{\sum |\vec{p}_i|}$$

where $\vec{p}_i$ is the momentum vector of particle i. The thrust axis $\vec{n}_\mathrm{T}$ is the unit vector which maximizes the above expression. The value of the thrust can vary between 0.5 and 1.0. The plane normal to $\vec{n}_\mathrm{T}$ divides space into two hemispheres, $S_\pm$, which are used in the following definitions.

Scaled heavy jet mass

The heavy jet mass, M_H, is defined [7] as

$$M_\mathrm{H} = \max[M_+, M_-] \, ,$$

where $M_\pm$ are the invariant masses in the two hemispheres, $S_\pm$,

$$M_\pm^2 = \left[\sum_{i\in S_\pm} p_i\right]^2$$

where p_i is the four-momentum of particle i. The scaled heavy jet mass, ρ_H, is defined as

$$\rho_\mathrm{H} = \frac{{M_\mathrm{H}}^2}{s} .$$

Jet broadening variables

These variables are defined [8,9] by computing in each hemisphere the quantity

$$B_\pm = \frac{\sum_{i\in S\pm} |\vec{p}_i \times \vec{n}_\mathrm{T}|}{2\sum_i |\vec{p}_i|}$$

in terms of which the total jet broadening, B_T, and wide jet broadening, B_W, are defined as

$$B_\mathrm{T} = B_+ + B_- \quad \text{and} \quad B_\mathrm{W} = \max(B_+, B_-) .$$

***C*-parameter**

The C-parameter is derived from the eigenvalues of the linearized momentum tensor [10]:

$$\Theta_{ij} = \frac{\sum_a p_a^i p_a^j / \mid \vec{p}_a \mid}{\sum_a \mid \vec{p}_a \mid} \quad i,j = 1,2,3 ;$$

where a runs over final state hadrons and i, j indicate components of vectors $\vec{p}_a$. With λ_1, λ_2 and λ_3 the eigenvalues of Θ, the C-parameter is defined as

$$C = 3(\lambda_1\lambda_2 + \lambda_2\lambda_3 + \lambda_3\lambda_1) .$$

Jet resolution parameter

Jets are reconstructed using the JADE algorithm [11]. The value of the "closeness variable" at which the classification of an event changes from 2-jet to 3-jet is called the 3-jet resolution parameter y_{23}^J.

Data and Monte Carlo Samples

The data discussed in this analysis correspond to an integrated luminosity of 602.2 pb^{-1}, collected during the years 1998–2000 at $\sqrt{s} \geq$ 189–207 GeV as detailed in Table 1. Only data corresponding to data-taking periods where all sub-detectors were fully operational are retained in this analysis.

The primary trigger for hadronic events requires a total energy greater than 15 GeV in the calorimeters. This trigger is in logical OR with a trigger using the barrel scintillation counters and with a charged-track trigger. The combined trigger efficiency for the selected hadronic events exceeds 99.9%.

The selection of $e^+e^- \to q\bar{q} \to$ *hadrons* events is based on the energy measured in the electromagnetic and hadron calorimeters. Energy clusters in the calorimeters are selected with a minimum energy of 100 MeV. The principal variables used to distinguish these hadronic events from background are the cluster multiplicity and energy imbalances. Energy clusters in the calorimeters are used to measure the total visible energy E_{vis}, and the energy imbalances parallel and perpendicular to the beam direction:

$$\begin{aligned} E_{\parallel} &= \left|\sum E\cos\theta\right| , \\ E_{\perp} &= \sqrt{\left(\sum E\sin\theta\sin\phi\right)^2 + \left(\sum E\sin\theta\cos\phi\right)^2} , \end{aligned}$$

respectively, where E is the energy of a cluster and θ and ϕ are its polar and azimuthal angles with respect to the beam direction.

Monte Carlo events are used to estimate the efficiency of the selection criteria and purity of the data sample. Monte Carlo events for the process $e^+e^- \to q\bar{q} \to$ *hadrons* are generated by the parton shower programs PYTHIA [12] for $\sqrt{s} = 189$ GeV and KK2f [13], which uses PYTHIA for hadronization, for the highest energies. QCD parton shower and fragmentation process are taken from JETSET 7.4 [14]. The generated events are passed through the L3 detector simulation [15]. The background events are simulated with PYTHIA and PHOJET [16] for hadron production in two-photon interactions, KORALZ [17] for $\tau^+\tau^-$ final state, BHAGENE [18] for Bhabha events, KORALW [19] for W-boson pair-production and PYTHIA for Z-boson pair-production.

Predictions of the parton shower models JETSET [14], HERWIG [20] and ARIADNE [21] are used to compare with the signal distributions. Parameters of these models are tuned with Z-peak data on global event shape [3].

Event Selection and Flavour Tagging

This analysis has two main sources of background. The first is the so called "radiative return" events, where initial state radiation results in a mass of the hadronic system close to the Z boson. The second is pair-production of W or Z bosons where one or both of the bosons decay hadronically. Additional background arises from hadron production in two-photon interaction and τ pair production. Events are first selected by requiring $E_{\mathrm{vis}}/\sqrt{s} > 0.7$, $E_{\perp}/E_{\mathrm{vis}} < 0.4$, number of clusters > 12, and at least one well-measured charged track. To reduce the radiative return background, events are rejected if they have a high-energy photon candidate, defined as a cluster in the electromagnetic calorimeter with at least 85% of its energy in a 15° cone and a total energy greater than $0.18\sqrt{s}$. Radiative return events, where an unobserved photon is emitted close to the beam axis, are reduced by requiring $\sqrt{s'/s} > 0.85$, where $\sqrt{s'}$ is determined from angles of the jets. To reject boson pair-production events where one of the bosons decays into leptons, events having an electron or muon with energy greater than 40 GeV are removed. Hadronic decays of boson pair events are rejected by:

1. forcing the event to a 4-jet topology using the Durham jet algorithm [22],
2. performing a kinematic fit imposing energy-momentum conservation,
3. applying cuts on the energies of the most- and the least-energetic jets and on the jet resolution parameter, y_{34}^{D}, at which the event classification changes from 3-jet to 4-jet.

Events are rejected if the energy of the most energetic jet is less than $0.4\sqrt{s}$, the ratio of the energy of the most energetic jet to the least energetic jet is less than 5, $y^{\mathrm{D}}_{34} > 0.007$, there are more than 40 clusters and more than 15 charged tracks, and $E_{\|} < 0.2E_{\mathrm{vis}}$ after the kinematic fit.

This selection removes 11.6% of the signal events, 98.1% of the radiative return events, 83.3% and 80.1%, respectively, of W-boson and Z-boson pair-production events. We select a total of about 13900 hadronic events with an efficiency of 88.3% and with a purity of better than 78.2%. The backgrounds due to radiative return, W-boson pairs, Z-boson pairs and hadron production in two-photon interaction are 5.7%, 12.3%, 1.0% and 2.6%, respectively. The remaining backgrounds are negligible. The integrated luminosity and the number of selected events for each energy point are summarized in Table 1.

Heavy (b) flavour events are separated from light (u, d, s, c) flavour events by using the characteristic decay properties of the b-hadrons. As the first step, the interaction vertex is estimated fill-by-fill by iteratively fitting all the good tracks measured in the detector during the fill. Measurements of all n tracks in the event contribute to a probability, $P^{[n]}$, that all tracks in the event originate from the interaction vertex. This probability is flat for zero lifetime of all produced particles but otherwise peaks at zero. A weighted discriminant is used: $B_{\mathrm{n}} = -\log P$, where $P = P^{[n]} \sum_{j=0}^{n-1} (-\log P^{[n]})^j / j!$ and $P^{[n]} = \prod_{j=1}^{n} P_j$ and P_j is the probability that track j originates from the primary vertex [23].

Figure 1 shows the distribution of the discriminant B_{n} for data as well as expectations from signal and background. A cut on this discriminant is made to distinguish events with b-quarks from events without. These two samples are called “b-events” and “non-b events” in the following. The non-b events are selected using $B_{\mathrm{n}} < 1.0$. The b-events are selected with a cut on $B_{\mathrm{n}} > 3.4$. A total of 440 b-events are selected with an efficiency of 26.2% and a purity of 75.2% while 6895 non-b events are selected with a selection efficiency of 75.5% and a purity of 72.7%.

Measurements

The distributions of event shape variables are measured at each energy point listed in Table 1. The data distributions are compared to a sum of the signal and the different background Monte Carlo distributions obtained using the same selection procedure and normalized to the integrated luminosity according to the Standard Model cross sections. For Monte Carlo events, these event shape variables are calculated before (particle level) and after (detector level) detector simulation. The calculation before detector simulation takes into account all stable charged and neutral particles. The measured distributions at detector level differ from the ones at particle level because of detector effects, limited acceptance and finite resolution.

After subtracting the background events the measured distributions are corrected for detector effects, acceptance and resolution, on a bin-by-bin basis by comparing the detector level results with the particle level results. In the extraction of flavour-tagged distributions, the effect of wrong-flavour contamination is corrected for by using a treatment similar to the Standard Model background subtraction.

The data are corrected for initial and final state photon radiation bin-by-bin using Monte Carlo distributions at particle level with and without radiation. Data at the different energy points are combined at the average centre-of-mass energy $\langle\sqrt{s}\rangle = 197$ GeV. Figures 2 and 3 show the measured distributions for event thrust and total jet broadening for all data, b-events and non-b events. The distributions are compared to predictions from signal and background Monte Carlo programs. There is generally good agreement between data and Monte Carlo particularly for the entire sample thus justifying the use of the latter to obtain the corrected distributions.

Systematic Uncertainties

The systematic uncertainties in the distribution of event shape variables arise mainly from uncertainties in the estimation of the detector corrections and the background levels. The uncertainty in detector correction is estimated by several independent checks:

- The definition of reconstructed objects used to calculate the observables is changed from calorimetric clusters only to a non-linear combination of charged tracks with calorimetric clusters.
- The effect of different particle densities in correcting the measured distributions is estimated by using a different signal Monte Carlo program, Herwig instead of Jetset or Pythia.
- The acceptance is reduced by restricting the events to the central part of the detector, $|\cos(\theta_T)| < 0.7$, where θ_T is the polar angle of the thrust axis relative to the beam axis.

The following systematic checks are made on the background estimations:

- An alternative criterion is applied to reject radiative return events based on a cut in the two dimensional plane of $E_{\|}/E_{\mathrm{vis}}$ and $E_{\mathrm{vis}}/\sqrt{s}$.
- The estimated background from two-photon interaction is varied by ±30% and is simulated by using the Phojet instead of the Pythia Monte Carlo program.
- The W-boson pair-production background is estimated from the KoralW Monte Carlo and subtracted from the data, while releasing the cut on 4-jet events which are no longer removed from the data.

Uncertainties due to detector corrections are between 7% and 10%, roughly 3 times larger than the uncertainty due to background estimation. The later are dominated in equal parts by uncertainties due to radiative return and W-boson pair-production. In the flavour-tagged cases, the background uncertainty is mainly due to contamination from the wrong flavour, between 3%–4% for the non-b events and 7%–10% for b-events.

The statistical component of the systematic uncertainty is negligible as the size of the Monte Carlo samples is more than 4 times, and sometimes even 10 times, larger than the size of the data sample. The final systematic uncertainty is taken as the sum in quadrature of all the contributions.

Results

The corrected distributions for the six chosen event shape distributions, thrust, scaled heavy jet mass, total and wide jet broadening, C-parameter and 3-jet resolution parameter for the Jade algorithm, are summarized in Tables 2–7 for $\langle\sqrt{s}\rangle = 197$ GeV. These tables also show the first and second moments of these distributions. The same six event shape distributions at $\sqrt{s} = 91.2$ GeV were previously measured as reported in reference [3].

Figures 4–9 show comparisons between data at $\langle\sqrt{s}\rangle = 197$ GeV and predictions of the parton shower models JETSET, HERWIG, ARIADNE for distributions of thrust, scaled heavy jet mass, total and wide jet broadening, C-parameter and the 3-jet JADE resolution parameter for all hadronic events, b-events and non-b events. The ratios of the event shape distributions for b- and non-b events are also shown together with predictions from parton shower models.

Generally a good agreement between data and the model predictions is observed. For the b-events in the 2-jet region the model predictions overestimate the data in particular for the thrust (Figure 4a), wide jet broadening (Figure 7a) and C-parameter distributions (Figure 8a).

Summary

Event shape distributions for hadronic events are studied from e^+e^- annihilation data collected by the L3 detector at LEP at $\langle\sqrt{s}\rangle = 197$ GeV. Flavour tagging is used to separate a b-quark enriched sample from a sample of lighter flavours.

The event shape distributions are well described by the parton shower models JETSET, HERWIG and ARIADNE for the total event sample. Some discrepancies are observed in the 2-jet region for the b-event sample.

Author List

The L3 Collaboration:

P.Achard,[20] O.Adriani,[17] M.Aguilar-Benitez,[25] J.Alcaraz,[25] G.Alemanni,[23] J.Allaby,[18] A.Aloisio,[29] M.G.Alviggi,[29] H.Anderhub,[49] V.P.Andreev,[6,34] F.Anselmo,[8] A.Arefiev,[28] T.Azemoon,[3] T.Aziz,[9] P.Bagnaia,[39] A.Bajo,[25] G.Baksay,[26] L.Baksay,[26] S.V.Baldew,[2] S.Banerjee,[9] Sw.Banerjee,[4] A.Barczyk,[49,47] R.Barillère,[18] P.Bartalini,[23] M.Basile,[8] N.Batalova,[46] R.Battiston,[33] A.Bay,[23] U.Becker,[13] F.Behner,[49] L.Bellucci,[17] R.Berbeco,[3] J.Berdugo,[25] P.Berges,[13] B.Bertucci,[33] B.L.Betev,[49] M.Biasini,[33] M.Biglietti,[29] A.Biland,[49] J.J.Blaising,[4] S.C.Blyth,[35] G.J.Bobbink,[2] A.Böhm,[1] L.Boldizsar,[12] B.Borgia,[39] S.Bottai,[17] D.Bourilkov,[49] M.Bourquin,[20] S.Braccini,[20] J.G.Branson,[41] F.Brochu,[4] J.D.Burger,[13] W.J.Burger,[33] X.D.Cai,[13] M.Capell,[13] G.Cara Romeo,[8] G.Carlino,[29] A.Cartacci,[17] J.Casaus,[25] F.Cavallari,[39] N.Cavallo,[36] C.Cecchi,[33] M.Cerrada,[25] M.Chamizo,[20] Y.H.Chang,[44] M.Chemarin,[24] A.Chen,[44] G.Chen,[7] G.M.Chen,[7] H.F.Chen,[22] H.S.Chen,[7] G.Chiefari,[29] L.Cifarelli,[40] F.Cindolo,[8] I.Clare,[13] R.Clare,[38] G.Coignet,[4] N.Colino,[25] S.Costantini,[39] B.de la Cruz,[25] S.Cucciarelli,[33] R.de Asmundis,[29] P.Déglon,[20] J.Debreczeni,[12] A.Degré,[4] K.Dehmelt,[26] K.Deiters,[47] D.della Volpe,[29] E.Delmeire,[20] P.Denes,[37] F.DeNotaristefani,[39] A.De Salvo,[49] M.Diemoz,[39] M.Dierckxsens,[2] C.Dionisi,[39] M.Dittmar,[49] A.Doria,[29] M.T.Dova,[10,♯] D.Duchesneau,[4] M.Duda,[1] B.Echenard,[20] A.Eline,[18] A.El Hage,[1] H.El Mamouni,[24] A.Engler,[35] F.J.Eppling,[13] P.Extermann,[20] M.A.Falagan,[25] S.Falciano,[39] A.Favara,[32] J.Fay,[24] O.Fedin,[34] M.Felcini,[49] T.Ferguson,[35] H.Fesefeldt,[1] E.Fiandrini,[33] J.H.Field,[20] F.Filthaut,[31] P.H.Fisher,[13] W.Fisher,[37] G.Forconi,[13] K.Freudenreich,[49] C.Furetta,[27] Yu.Galaktionov,[28,13] S.N.Ganguli,[9] P.Garcia-Abia,[25] M.Gataullin,[32] S.Gentile,[39] S.Giagu,[39] Z.F.Gong,[22] G.Grenier,[24] O.Grimm,[49] M.W.Gruenewald,[16] V.K.Gupta,[37] A.Gurtu,[9] L.J.Gutay,[46] D.Haas,[5] D.Hatzifotiadou,[8] T.Hebbeker,[1] A.Hervé,[18] J.Hirschfelder,[35] H.Hofer,[49] M.Hohlmann,[26] G.Holzner,[49] S.R.Hou,[44] B.N.Jin,[7] P.Jindal,[14] L.W.Jones,[3] P.de Jong,[2] I.Josa-Mutuberría,[25] M.Kaur,[14] M.N.Kienzle-Focacci,[20] J.K.Kim,[43] J.Kirkby,[18] W.Kittel,[31] A.Klimentov,[13,28] A.C.König,[31] M.Kopal,[46] V.Koutsenko,[13,28] M.Kräber,[49] R.W.Kraemer,[35] A.Krüger,[48] A.Kunin,[13] P.Ladron de Guevara,[25] I.Laktineh,[24] G.Landi,[17] M.Lebeau,[18] A.Lebedev,[13] P.Lebrun,[24] P.Lecomte,[49] P.Lecoq,[18] P.Le Coultre,[49] J.M.Le Goff,[18] R.Leiste,[48] M.Levtchenko,[27] P.Levtchenko,[34] C.Li,[22] S.Likhoded,[48] C.H.Lin,[44] W.T.Lin,[44] F.L.Linde,[2] L.Lista,[29] Z.A.Liu,[7] W.Lohmann,[48] E.Longo,[39] Y.S.Lu,[7] C.Luci,[39] L.Luminari,[39] W.Lustermann,[49] W.G.Ma,[22] L.Malgeri,[18] A.Malinin,[28] C.Maña,[25] J.Mans,[37] J.P.Martin,[24] F.Marzano,[39] K.Mazumdar,[9] R.R.McNeil,[6] S.Mele,[18,29] L.Merola,[29] M.Meschini,[17] W.J.Metzger,[31] A.Mihul,[11] H.Milcent,[18] G.Mirabelli,[39] J.Mnich,[1] G.B.Mohanty,[9] G.S.Muanza,[24] A.J.M.Muijs,[2] M.Musy,[39] S.Nagy,[15] S.Natale,[20] M.Napolitano,[29] F.Nessi-Tedaldi,[49] H.Newman,[32] A.Nisati,[39] T.Novak,[31] H.Nowak,[48] R.Ofierzynski,[49] G.Organtini,[39] I.Pal,[46]C.Palomares,[25] P.Paolucci,[29] R.Paramatti,[39] G.Passaleva,[17] S.Patricelli,[29] T.Paul,[10] M.Pauluzzi,[33] C.Paus,[13] F.Pauss,[49] M.Pedace,[39] S.Pensotti,[27] D.Perret-Gallix,[4] D.Piccolo,[29] F.Pierella,[8] M.Pieri,[41] M.Pioppi,[33] P.A.Piroué,[37] E.Pistolesi,[27] V.Plyaskin,[28] M.Pohl,[20] V.Pojidaev,[17] J.Pothier,[18] D.Prokofiev,[34] G.Rahal-Callot,[49] M.A.Rahaman,[9] P.Raics,[15] N.Raja,[9] R.Ramelli,[49] P.G.Rancoita,[27] R.Ranieri,[17] A.Raspereza,[48] P.Razis,[30] S.Rembeczki,[26] D.Ren,[49] M.Rescigno,[39] S.Reucroft,[10] S.Riemann,[48] K.Riles,[3] B.P.Roe,[3] L.Romero,[25] A.Rosca,[48] C.Rosemann,[1] C.Rosenbleck,[1] S.Rosier-Lees,[4] S.Roth,[1] J.A.Rubio,[18] G.Ruggiero,[17] H.Rykaczewski,[49] A.Sakharov,[49] S.Saremi,[6] S.Sarkar,[39] J.Salicio,[18] E.Sanchez,[25] C.Schäfer,[18] V.Schegelsky,[34] H.Schopper,[21] D.J.Schotanus,[31] C.Sciacca,[29] L.Servoli,[33] S.Shevchenko,[32] N.Shivarov,[42] V.Shoutko,[13] E.Shumilov,[28] A.Shvorob,[32] D.Son,[43] C.Souga,[24] P.Spillantini,[17] M.Steuer,[13] D.P.Stickland,[37] B.Stoyanov,[42] A.Straessner,[20] K.Sudhakar,[9] G.Sultanov,[42] L.Z.Sun,[22] S.Sushkov,[1] H.Suter,[49] J.D.Swain,[10] Z.Szillasi,[26,¶] X.W.Tang,[7] P.Tarjan,[15] L.Tauscher,[5] L.Taylor,[10] B.Tellili,[24] D.Teyssier,[24] C.Timmermans,[31] Samuel C.C.Ting,[13] S.M.Ting,[13] S.C.Tonwar,[9] J.Tóth,[12] C.Tully,[37] K.L.Tung,[7]J.Ulbricht,[49] E.Valente,[39] R.T.Van de Walle,[31] R.Vasquez,[46] G.Vesztergombi,[12] I.Vetlitsky,[28] G.Viertel,[49] M.Vivargent,[4] S.Vlachos,[5] I.Vodopianov,[26] H.Vogel,[35] H.Vogt,[48] I.Vorobiev,[35,28] A.A.Vorobyov,[34] M.Wadhwa,[5] Q.Wang[31] X.L.Wang,[22] Z.M.Wang,[22] M.Weber,[18] S.Wynhoff,[37,†] L.Xia,[32] Z.Z.Xu,[22] J.Yamamoto,[3] B.Z.Yang,[22] C.G.Yang,[7] H.J.Yang,[3] M.Yang,[7] S.C.Yeh,[45] An.Zalite,[34] Yu.Zalite,[34] Z.P.Zhang,[22] J.Zhao,[22] G.Y.Zhu,[7] R.Y.Zhu,[32] H.L.Zhuang,[7] A.Zichichi,[8,18,19] B.Zimmermann,[49] M.Zöller.[1]

1 III. Physikalisches Institut, RWTH, D-52056 Aachen, Germany§
2 National Institute for High Energy Physics, NIKHEF, and University of Amsterdam, NL-1009 DB Amsterdam, The Netherlands
3 University of Michigan, Ann Arbor, MI 48109, USA
4 Laboratoire d'Annecy-le-Vieux de Physique des Particules, LAPP,IN2P3-CNRS, BP 110, F-74941 Annecy-le-Vieux CEDEX, France
5 Institute of Physics, University of Basel, CH-4056 Basel, Switzerland
6 Louisiana State University, Baton Rouge, LA 70803, USA
7 Institute of High Energy Physics, IHEP, 100039 Beijing, China△
8 University of Bologna and INFN-Sezione di Bologna, I-40126 Bologna, Italy
9 Tata Institute of Fundamental Research, Mumbai (Bombay) 400 005, India
10 Northeastern University, Boston, MA 02115, USA
11 Institute of Atomic Physics and University of Bucharest, R-76900 Bucharest, Romania
12 Central Research Institute for Physics of the Hungarian Academy of Sciences, H-1525 Budapest 114, Hungary‡
13 Massachusetts Institute of Technology, Cambridge, MA 02139, USA
14 Panjab University, Chandigarh 160 014, India
15 KLTE-ATOMKI, H-4010 Debrecen, Hungary¶
16 UCD School of Physics, University College Dublin, Belfield, Dublin 4, Ireland
17 INFN Sezione di Firenze and University of Florence, I-50125 Florence, Italy
18 European Laboratory for Particle Physics, CERN, CH-1211 Geneva 23, Switzerland
19 World Laboratory, FBLJA Project, CH-1211 Geneva 23, Switzerland
20 University of Geneva, CH-1211 Geneva 4, Switzerland
21 University of Hamburg, D-22761 Hamburg, Germany
22 Chinese University of Science and Technology, USTC, Hefei, Anhui 230 029, China△
23 University of Lausanne, CH-1015 Lausanne, Switzerland
24 Institut de Physique Nucléaire de Lyon, IN2P3-CNRS,Université Claude Bernard, F-69622 Villeurbanne, France
25 Centro de Investigaciones Energéticas, Medioambientales y Tecnológicas, CIEMAT, E-28040 Madrid, Spain♭
26 Florida Institute of Technology, Melbourne, FL 32901, USA
27 INFN-Sezione di Milano, I-20133 Milan, Italy
28 Institute of Theoretical and Experimental Physics, ITEP, Moscow, Russia
29 INFN-Sezione di Napoli and University of Naples, I-80125 Naples, Italy
30 Department of Physics, University of Cyprus, Nicosia, Cyprus
31 Radboud University and NIKHEF, NL-6525 ED Nijmegen, The Netherlands
32 California Institute of Technology, Pasadena, CA 91125, USA
33 INFN-Sezione di Perugia and Università Degli Studi di Perugia, I-06100 Perugia, Italy
34 Nuclear Physics Institute, St. Petersburg, Russia
35 Carnegie Mellon University, Pittsburgh, PA 15213, USA
36 INFN-Sezione di Napoli and University of Potenza, I-85100 Potenza, Italy
37 Princeton University, Princeton, NJ 08544, USA
38 University of Californa, Riverside, CA 92521, USA
39 INFN-Sezione di Roma and University of Rome, "La Sapienza", I-00185 Rome, Italy
40 University and INFN, Salerno, I-84100 Salerno, Italy
41 University of California, San Diego, CA 92093, USA
42 Bulgarian Academy of Sciences, Central Lab. of Mechatronics and Instrumentation, BU-1113 Sofia, Bulgaria
43 The Center for High Energy Physics, Kyungpook National University, 702-701 Taegu, Republic of Korea
44 National Central University, Chung-Li, Taiwan, China
45 Department of Physics, National Tsing Hua University, Taiwan, China
46 Purdue University, West Lafayette, IN 47907, USA
47 Paul Scherrer Institut, PSI, CH-5232 Villigen, Switzerland
48 DESY, D-15738 Zeuthen, Germany
49 Eidgenössische Technische Hochschule, ETH Zürich, CH-8093 Zürich, Switzerland
§ Supported by the German Bundesministerium für Bildung, Wissenschaft, Forschung und Technologie.
‡ Supported by the Hungarian OTKA fund under contract numbers T019181, F023259 and T037350.
¶ Also supported by the Hungarian OTKA fund under contract number T026178.
♭ Supported also by the Comisión Interministerial de Ciencia y Tecnología.
♯ Also supported by CONICET and Universidad Nacional de La Plata, CC 67, 1900 La Plata, Argentina.
△ Supported by the National Natural Science Foundation of China.
† Deceased.

References

[1] H. Fritzsch, M. Gell-Mann and H. Leytwyler, Phys. Lett. **B47** (1973) 365;
S. Weinberg, Phys. Rev. Lett. **31** (1973) 494;
D. J. Gross and F. Wilczek, Phys. Rev. Lett. **30** (1973) 1343;
D. J. Gross and F. Wilczek, Phys. Rev. **D8** (1973) 3633;
H. D. Politzer, Phys. Rev. Lett. **30** (1973) 1346..

[2] R. K. Ellis, W. J. Stirling and B. R. Webber, *QCD and Collider Physics*, Cambridge University Press (1996); and references therein..

[3] L3 Collaboration, P. Achard *et al.*, Physics Reports **399** (2004) 71..

[4] Aleph Collaboration, A. Heister *et al.*, European Physics Journal **C35** (2004) 457;
Delphi Collaboration: J. Abdallah *et al.*, European Physics Journal **C37** (2004) 1;
Opal Collaboration, G. Abbiendi *et al.*, European Physics Journal **C40** (2005) 287;
G. Dissertori *et al.*, JHEP **02** (2008) 040..

[5] Opal Collaboration, R. Akers *et al.*, Z. Physik **C65** (1995) 31..

[6] S. Brandt *et al.*, Phys. Lett. **12** (1964) 57;
E. Fahri, Phys. Rev. Lett. **39** (1977) 1587..

[7] T. Chandramohan and L. Clavelli, Nucl. Phys. **B184** (1981) 365;
Mark-II Collaboration, A. Peterson *et al.*, Phys. Rev. **D37** (1998) 1;
Tasso Collaboration, D. P. Barber *et al.*, Z. Physik **C45** (1989) 11..

[8] S. Catani *et al.*, Phys. Lett. **B295** (1991) 269..

[9] Yu. L. Dokshitzer *et al.*, Journal of High Energy Physics **01** (1998) 11..

[10] G. Parisi, Phys. Lett. **B74** (1978) 65;
J. F. Donoghue, F. E. Low and S. Y. Pi, Phys. Rev. **D20** (1979) 2759..

[11] Jade Collaboration, W. Bartel *et al.*, Z. Physik **C33** (1986) 23;
Jade Collaboration, S. Bethke *et al.*, Phys. Lett. **B213** (1988) 235..

[12] Pythia 5.7 Monte Carlo Program:
T. Sjöstrand, CERN-TH-7112/93 (1993), revised August 1995..

[13] Kk2f 4.14 Monte Carlo Program:
S. Jadach, B. F. L. Ward and Z. Wąs, Comp. Phys. Comm. **130** (2000) 260;
S. Jadach, B. F. L. Ward and Z. Wąs, Phys. Rev. **D63** (2001) 113009..

[14] Jetset 7.4 Monte Carlo Program:
T. Sjöstrand, Comp. Phys. Comm. **82** (1994) 74..

[15] The L3 detector simulation is based on GEANT Version 3.15.
See R. Brun *et al.*, “GEANT 3”, CERN DD/EE/84-1 (Revised), September 1987.
The GHEISHA program (H. Fesefeldt, RWTH Aachen Report PITHA 85/02 (1985)) is used to simulate hadronic interactions..

[16] Phojet Monte Carlo Program:
R. Engel, Z. Physik **C66** (1995) 1459;
R. Engel, J. Ranft and S. Roesler, Phys. Rev. **D52** (1995) 1459..

[17] KoralZ Monte Carlo Program:
S. Jadach, B. F. L. Ward and Z. Wąs, Comp. Phys. Comm. **79** (1994) 503..

[18] Bhagene Monte Carlo Program:
J. H. Field, Phys. Lett. **B323** (1994) 432;
J. H. Field and T. Riemann, Comp. Phys. Comm. **94** (1996) 53..

[19] KoralW Monte Carlo Program:
M. Skrzypek *et al.*, Comp. Phys. Comm. **94** (1996) 216;
M. Skrzypek *et al.*, Phys. Lett. **B372** (1996) 289..

[20] Herwig 5.9 Monte Carlo Program:
G. Marchesini and B. R. Webber, Nucl. Phys. **B310** (1988) 461;
I. G. Knowles, Nucl. Phys. **B310** (1988) 571;
G. Marchesini *et al.*, Comp. Phys. Comm. **67** (1992) 465..

[21] Ariadne Monte Carlo Program:
L. Lönnblad, Comp. Phys. Comm. **71** (1992) 15..

[22] Yu. L. Dokshitzer, Contribution to the workshop on Jets at LEP and HERA (1990);
N. Brown and W. J. Stirling, Rutherford Preprint RAL-91-049;
S. Catani *et al.*, Phys. Lett. **B269** (1991) 432;
S. Bethke *et al.*, Nucl. Phys. **B370** (1992) 310..

[23] L3 Collaboration, M. Acciarri *et al.*, Phys. Lett. **B411** (1997) 373..

$\sqrt{s}$ (GeV)	Integrated Luminosity (pb^{-1})	Selection Efficiency (%)	Sample Purity (%)	Selected events
188.6	175.1	87.7	80.9	4473
191.6	29.4	87.8	80.1	720
195.5	83.4	88.4	78.6	1884
199.5	81.2	88.5	77.5	1835
201.7	36.5	89.0	77.0	817
205.1	70.5	88.8	75.6	1496
206.5	126.2	88.9	75.3	2688
197.0	602.2	88.3	78.2	13913

Table 1: Summary of integrated luminosity and number of selected hadronic events at the different energies. The last line corresponds to the average $\langle\sqrt{s}\rangle$ and the total sample.

Thrust (T)	$\frac{1}{\sigma}\cdot\frac{\mathrm{d}\sigma}{\mathrm{d}T}$ (All)	$\frac{1}{\sigma}\cdot\frac{\mathrm{d}\sigma}{\mathrm{d}T}$ (Non-b)	Thrust (T)	$\frac{1}{\sigma}\cdot\frac{\mathrm{d}\sigma}{\mathrm{d}T}$ (b)
0.500−0.600	0.00 ± 0.00 ± 0.00	0.00 ± 0.00 ± 0.00	0.500−0.600	0.00 ± 0.00 ± 0.00
0.600−0.650	0.01 ± 0.01 ± 0.02	0.01 ± 0.01 ± 0.04	0.600−0.650	0.00 ± 0.00 ± 0.00
0.650−0.700	0.13 ± 0.06 ± 0.06	0.26 ± 0.12 ± 0.11	0.650−0.700	0.04 ± 0.04 ± 0.03
0.700−0.750	0.19 ± 0.06 ± 0.04	0.42 ± 0.13 ± 0.15	0.700−0.750	0.63 ± 0.31 ± 0.36
0.750−0.800	0.56 ± 0.08 ± 0.11	0.67 ± 0.15 ± 0.15	0.750−0.800	0.62 ± 0.43 ± 0.37
0.800−0.825	0.80 ± 0.10 ± 0.11	0.88 ± 0.18 ± 0.18	0.800−0.850	1.14 ± 0.45 ± 0.59
0.825−0.850	1.05 ± 0.10 ± 0.08	1.23 ± 0.20 ± 0.18	0.850−0.900	2.95 ± 0.70 ± 0.44
0.850−0.875	1.62 ± 0.11 ± 0.17	1.76 ± 0.19 ± 0.26	0.900−0.925	3.43 ± 0.91 ± 1.09
0.875−0.900	1.72 ± 0.10 ± 0.21	1.60 ± 0.17 ± 0.32	0.925−0.950	5.02 ± 1.05 ± 0.45
0.900−0.925	3.03 ± 0.12 ± 0.23	3.24 ± 0.22 ± 0.19	0.950−0.975	8.97 ± 1.43 ± 0.97
0.925−0.950	4.72 ± 0.14 ± 0.23	5.09 ± 0.27 ± 0.38	0.975−1.000	11.83 ± 1.94 ± 0.70
0.950−0.975	9.24 ± 0.19 ± 0.22	8.95 ± 0.37 ± 0.24		
0.975−1.000	16.04 ± 0.25 ± 1.09	14.54 ± 0.56 ± 1.11		
First Moment	0.943 ±0.010 ±0.004	0.935 ±0.020 ±0.003		0.927 ±0.072 ±0.010
Second Moment	0.893 ±0.010 ±0.007	0.879 ±0.021 ±0.006		0.865 ±0.072 ±0.016

Table 2: Differential distribution and first and second moments for event thrust at $\langle\sqrt{s}\rangle = 197$ GeV for all, non-b and b events.

ρ_H	$\frac{1}{\sigma}\cdot\frac{\mathrm{d}\sigma}{\mathrm{d}\rho_\mathrm{H}}$ (All)	$\frac{1}{\sigma}\cdot\frac{\mathrm{d}\sigma}{\mathrm{d}\rho_\mathrm{H}}$ (Non-b)	ρ_H	$\frac{1}{\sigma}\cdot\frac{\mathrm{d}\sigma}{\mathrm{d}\rho_\mathrm{H}}$ (b)
0.000−0.015	20.31 ± 0.33 ± 1.68	18.24 ± 0.74 ± 1.76	0.000−0.015	15.10 ± 2.49 ± 1.16
0.015−0.030	15.93 ± 0.34 ± 0.61	15.60 ± 0.69 ± 0.73	0.015−0.030	15.32 ± 2.71 ± 0.95
0.030−0.045	8.72 ± 0.26 ± 0.19	8.58 ± 0.47 ± 0.44	0.030−0.045	7.77 ± 1.93 ± 1.72
0.045−0.060	5.12 ± 0.21 ± 0.41	5.18 ± 0.38 ± 0.56	0.045−0.060	4.95 ± 1.46 ± 1.11
0.060−0.075	3.59 ± 0.18 ± 0.42	3.74 ± 0.33 ± 0.66	0.060−0.075	4.39 ± 1.39 ± 0.45
0.075−0.090	2.76 ± 0.17 ± 0.14	3.05 ± 0.31 ± 0.14	0.075−0.090	4.34 ± 1.57 ± 0.51
0.090−0.105	2.22 ± 0.16 ± 0.27	2.37 ± 0.28 ± 0.42	0.090−0.120	3.46 ± 0.91 ± 0.53
0.105−0.120	1.89 ± 0.16 ± 0.25	1.96 ± 0.28 ± 0.32	0.120−0.150	1.69 ± 0.60 ± 0.97
0.120−0.150	1.11 ± 0.10 ± 0.12	1.22 ± 0.18 ± 0.16	0.150−0.180	0.95 ± 0.69 ± 0.45
0.150−0.180	0.75 ± 0.10 ± 0.06	0.96 ± 0.18 ± 0.16	0.180−0.210	0.49 ± 0.40 ± 0.49
0.180−0.210	0.51 ± 0.09 ± 0.11	0.63 ± 0.17 ± 0.17	0.210−0.240	0.21 ± 0.26 ± 0.21
0.210−0.240	0.27 ± 0.08 ± 0.06	0.39 ± 0.14 ± 0.13	0.240−0.270	0.32 ± 0.23 ± 0.17
0.240−0.270	0.23 ± 0.07 ± 0.04	0.41 ± 0.15 ± 0.11	0.270−0.300	0.26 ± 0.15 ± 0.10
0.270−0.300	0.17 ± 0.06 ± 0.05	0.37 ± 0.16 ± 0.14		
First Moment	0.046 ±0.001 ±0.003	0.053 ±0.002 ±0.003		0.057 ±0.005 ±0.006
Second Moment	0.005 ±0.001 ±0.001	0.006 ±0.001 ±0.001		0.006 ±0.001 ±0.001

Table 3: Differential distribution and first and second moments for scaled heavy jet mass at $\langle\sqrt{s}\rangle$ = 197 GeV for all, non-b and b events.

B_T	$\frac{1}{\sigma}\cdot\frac{\mathrm{d}\sigma}{\mathrm{d}B_\mathrm{T}}$ (All)	$\frac{1}{\sigma}\cdot\frac{\mathrm{d}\sigma}{\mathrm{d}B_\mathrm{T}}$ (Non-b)	B_T	$\frac{1}{\sigma}\cdot\frac{\mathrm{d}\sigma}{\mathrm{d}B_\mathrm{T}}$ (b)
0.000−0.020	0.75 ± 0.06 ± 0.30	0.68 ± 0.11 ± 0.37	0.000−0.020	0.20 ± 0.20 ± 0.29
0.020−0.040	8.61 ± 0.21 ± 0.61	8.17 ± 0.50 ± 0.71	0.020−0.040	4.80 ± 1.30 ± 0.68
0.040−0.060	10.10 ± 0.22 ± 0.41	9.15 ± 0.48 ± 0.51	0.040−0.060	8.03 ± 1.84 ± 1.08
0.060−0.080	7.50 ± 0.19 ± 0.16	6.73 ± 0.37 ± 0.18	0.060−0.080	7.47 ± 1.53 ± 0.64
0.080−0.100	5.58 ± 0.16 ± 0.18	6.03 ± 0.33 ± 0.37	0.080−0.100	5.85 ± 1.27 ± 0.70
0.100−0.120	4.17 ± 0.15 ± 0.18	4.18 ± 0.27 ± 0.39	0.100−0.120	4.83 ± 1.26 ± 0.91
0.120−0.140	3.22 ± 0.13 ± 0.22	3.37 ± 0.24 ± 0.46	0.120−0.140	4.15 ± 1.12 ± 0.54
0.140−0.160	2.43 ± 0.12 ± 0.19	2.43 ± 0.23 ± 0.17	0.140−0.160	3.62 ± 1.05 ± 1.20
0.160−0.180	2.01 ± 0.12 ± 0.16	2.27 ± 0.22 ± 0.16	0.160−0.200	2.27 ± 0.67 ± 0.47
0.180−0.200	1.54 ± 0.12 ± 0.19	1.46 ± 0.22 ± 0.22	0.200−0.240	1.28 ± 0.63 ± 0.49
0.200−0.240	1.24 ± 0.10 ± 0.12	1.52 ± 0.19 ± 0.22	0.240−0.280	1.58 ± 0.72 ± 0.40
0.240−0.280	0.53 ± 0.10 ± 0.15	0.63 ± 0.18 ± 0.17	0.280−0.320	0.30 ± 0.21 ± 0.21
0.280−0.320	0.16 ± 0.07 ± 0.07	0.50 ± 0.14 ± 0.18	0.320−0.360	0.10 ± 0.10 ± 0.07
0.320−0.360	0.11 ± 0.05 ± 0.06	0.12 ± 0.07 ± 0.13		
0.360−0.400	0.01 ± 0.01 ± 0.01	0.01 ± 0.01 ± 0.01		
First Moment	0.093 ±0.001 ±0.004	0.100 ±0.002 ±0.004		0.114 ±0.007 ±0.008
Second Moment	0.013 ±0.001 ±0.001	0.015 ±0.001 ±0.001		0.018 ±0.002 ±0.003

Table 4: Differential distribution and first and second moments for total jet broadening at $\langle\sqrt{s}\rangle$ = 197 GeV for all, non-b and b events.

B_{W}	$\frac{1}{\sigma}\cdot\frac{\mathrm{d}\sigma}{\mathrm{d}B_{\mathrm{W}}}$ (All)	$\frac{1}{\sigma}\cdot\frac{\mathrm{d}\sigma}{\mathrm{d}B_{\mathrm{W}}}$ (Non-b)	B_{W}	$\frac{1}{\sigma}\cdot\frac{\mathrm{d}\sigma}{\mathrm{d}B_{\mathrm{W}}}$ (b)
0.000−0.015	2.57 ± 0.12 ± 0.55	2.39 ± 0.27 ± 0.78	0.000−0.015	1.02 ± 0.51 ± 0.73
0.015−0.030	14.86 ± 0.32 ± 0.92	13.29 ± 0.72 ± 0.76	0.015−0.030	12.33 ± 2.56 ± 1.19
0.030−0.045	12.25 ± 0.27 ± 0.80	11.28 ± 0.59 ± 1.07	0.030−0.045	8.81 ± 1.91 ± 1.18
0.045−0.060	8.61 ± 0.24 ± 0.27	8.74 ± 0.49 ± 0.43	0.045−0.060	9.78 ± 2.00 ± 1.45
0.060−0.075	6.49 ± 0.21 ± 0.25	6.87 ± 0.42 ± 0.49	0.060−0.075	6.70 ± 1.72 ± 0.95
0.075−0.090	5.06 ± 0.20 ± 0.27	5.19 ± 0.36 ± 0.19	0.075−0.090	4.46 ± 1.30 ± 0.63
0.090−0.105	3.53 ± 0.17 ± 0.40	3.53 ± 0.31 ± 0.63	0.090−0.105	2.68 ± 0.98 ± 1.33
0.105−0.120	3.03 ± 0.17 ± 0.19	3.36 ± 0.31 ± 0.25	0.105−0.120	7.14 ± 1.87 ± 2.32
0.120−0.135	2.24 ± 0.16 ± 0.36	2.45 ± 0.29 ± 0.31	0.120−0.150	2.19 ± 0.74 ± 0.67
0.135−0.150	2.10 ± 0.16 ± 0.26	2.16 ± 0.30 ± 0.38	0.150−0.180	1.50 ± 0.64 ± 0.77
0.150−0.180	1.31 ± 0.11 ± 0.21	1.49 ± 0.19 ± 0.24	0.180−0.210	1.68 ± 0.67 ± 0.55
0.180−0.210	0.94 ± 0.11 ± 0.07	1.10 ± 0.19 ± 0.17	0.210−0.240	0.59 ± 0.49 ± 0.25
0.210−0.240	0.37 ± 0.10 ± 0.10	0.53 ± 0.17 ± 0.22	0.240−0.270	0.79 ± 0.39 ± 0.36
0.240−0.270	0.27 ± 0.07 ± 0.04	0.42 ± 0.14 ± 0.13	0.270−0.300	0.13 ± 0.13 ± 0.10
0.270−0.300	0.07 ± 0.03 ± 0.03	0.16 ± 0.06 ± 0.04		
First Moment	0.068 ±0.001 ±0.003	0.073 ±0.002 ±0.003		0.083 ±0.005 ±0.006
Second Moment	0.007 ±0.001 ±0.001	0.009 ±0.001 ±0.001		0.010 ±0.001 ±0.001

Table 5: Differential distribution and first and second moments for wide jet broadening at $\langle\sqrt{s}\rangle$ = 197 GeV for all, non-b and b events.

C-parameter	$\frac{1}{\sigma}\cdot\frac{\mathrm{d}\sigma}{\mathrm{d}C}$ (All)	$\frac{1}{\sigma}\cdot\frac{\mathrm{d}\sigma}{\mathrm{d}C}$ (Non-b)	C-parameter	$\frac{1}{\sigma}\cdot\frac{\mathrm{d}\sigma}{\mathrm{d}C}$ (b)
0.000−0.050	1.98 ± 0.07 ± 0.21	1.66 ± 0.13 ± 0.29	0.000−0.050	1.68 ± 0.48 ± 0.37
0.050−0.100	4.80 ± 0.10 ± 0.29	4.45 ± 0.22 ± 0.23	0.050−0.100	2.82 ± 0.68 ± 0.40
0.100−0.150	3.10 ± 0.08 ± 0.13	2.84 ± 0.16 ± 0.22	0.100−0.150	3.21 ± 0.64 ± 0.29
0.150−0.200	1.95 ± 0.06 ± 0.07	1.92 ± 0.12 ± 0.18	0.150−0.200	2.18 ± 0.52 ± 0.48
0.200−0.250	1.64 ± 0.06 ± 0.06	1.66 ± 0.11 ± 0.08	0.200−0.250	1.45 ± 0.42 ± 0.43
0.250−0.300	1.23 ± 0.05 ± 0.05	1.34 ± 0.10 ± 0.14	0.250−0.300	1.49 ± 0.41 ± 0.32
0.300−0.350	0.97 ± 0.05 ± 0.04	0.96 ± 0.08 ± 0.11	0.300−0.350	1.12 ± 0.33 ± 0.19
0.350−0.400	0.85 ± 0.05 ± 0.09	0.95 ± 0.09 ± 0.09	0.350−0.400	1.04 ± 0.36 ± 0.40
0.400−0.450	0.64 ± 0.04 ± 0.04	0.74 ± 0.08 ± 0.07	0.400−0.500	0.72 ± 0.23 ± 0.16
0.450−0.500	0.59 ± 0.04 ± 0.05	0.53 ± 0.07 ± 0.07	0.500−0.600	0.80 ± 0.26 ± 0.18
0.500−0.600	0.48 ± 0.03 ± 0.05	0.53 ± 0.06 ± 0.07	0.600−0.700	0.34 ± 0.19 ± 0.14
0.600−0.700	0.41 ± 0.04 ± 0.03	0.47 ± 0.07 ± 0.09	0.700−0.850	0.44 ± 0.16 ± 0.14
0.700−0.850	0.15 ± 0.03 ± 0.03	0.31 ± 0.07 ± 0.05		
0.850−1.000	0.01 ± 0.01 ± 0.01	0.01 ± 0.01 ± 0.01		
First Moment	0.222 ±0.004 ±0.014	0.248 ±0.007 ±0.011		0.271 ±0.019 ±0.028
Second Moment	0.084 ±0.003 ±0.010	0.104 ±0.006 ±0.008		0.117 ±0.015 ±0.026

Table 6: Differential distribution and first and second moments for C-parameter at $\langle\sqrt{s}\rangle$ = 197 GeV for all, non-b and b events.

y_{23}^{J}	$\frac{1}{\sigma}\cdot\frac{\mathrm{d}\sigma}{\mathrm{d}y_{23}^{\mathrm{J}}}$ (All)	$\frac{1}{\sigma}\cdot\frac{\mathrm{d}\sigma}{\mathrm{d}y_{23}^{\mathrm{J}}}$ (Non-b)	y_{23}^{J}	$\frac{1}{\sigma}\cdot\frac{\mathrm{d}\sigma}{\mathrm{d}y_{23}^{\mathrm{J}}}$ (b)
0.000−0.012	37.89 ± 0.62 ± 3.70	33.51 ± 1.30 ± 3.25	0.000−0.012	29.89 ± 4.75 ± 4.44
0.012−0.024	12.82 ± 0.31 ± 0.75	13.47 ± 0.65 ± 0.81	0.012−0.024	11.72 ± 2.48 ± 0.96
0.024−0.036	7.04 ± 0.24 ± 0.56	7.34 ± 0.47 ± 0.58	0.024−0.036	6.41 ± 1.68 ± 1.03
0.036−0.048	4.93 ± 0.20 ± 0.47	5.18 ± 0.40 ± 0.54	0.036−0.048	6.03 ± 1.62 ± 1.66
0.048−0.060	3.63 ± 0.18 ± 0.49	3.82 ± 0.35 ± 0.74	0.048−0.060	4.07 ± 1.24 ± 1.15
0.060−0.072	2.73 ± 0.16 ± 0.35	3.21 ± 0.32 ± 0.37	0.060−0.072	4.19 ± 1.33 ± 0.95
0.072−0.084	2.12 ± 0.15 ± 0.26	2.20 ± 0.28 ± 0.32	0.072−0.084	1.54 ± 0.71 ± 0.55
0.084−0.096	2.01 ± 0.15 ± 0.24	2.29 ± 0.27 ± 0.34	0.084−0.096	1.91 ± 1.04 ± 0.57
0.096−0.108	1.66 ± 0.14 ± 0.20	1.97 ± 0.27 ± 0.24	0.096−0.120	2.22 ± 0.74 ± 0.62
0.108−0.120	1.14 ± 0.13 ± 0.31	1.14 ± 0.23 ± 0.30	0.120−0.144	1.67 ± 0.68 ± 0.80
0.120−0.144	1.26 ± 0.10 ± 0.11	1.39 ± 0.18 ± 0.13	0.144−0.168	1.74 ± 0.74 ± 0.75
0.144−0.168	0.69 ± 0.09 ± 0.11	0.82 ± 0.17 ± 0.15	0.168−0.204	0.89 ± 0.45 ± 0.50
0.168−0.204	0.47 ± 0.08 ± 0.08	0.72 ± 0.14 ± 0.18	0.204−0.252	0.55 ± 0.31 ± 0.22
0.204−0.252	0.31 ± 0.06 ± 0.06	0.41 ± 0.12 ± 0.10	0.252−0.300	0.35 ± 0.19 ± 0.15
0.252−0.300	0.21 ± 0.05 ± 0.04	0.24 ± 0.08 ± 0.08		
First Moment	0.044 ±0.001 ±0.003	0.048 ±0.002 ±0.003		0.060 ±0.006 ±0.008
Second Moment	0.005 ±0.001 ±0.001	0.006 ±0.001 ±0.001		0.008 ±0.001 ±0.002

Table 7: Differential distribution and first and second moments for 3-jet resolution parameter (y_{23}^{J})in JADE algorithm at $\langle\sqrt{s}\rangle$ = 197 GeV for all, non-b and b events.

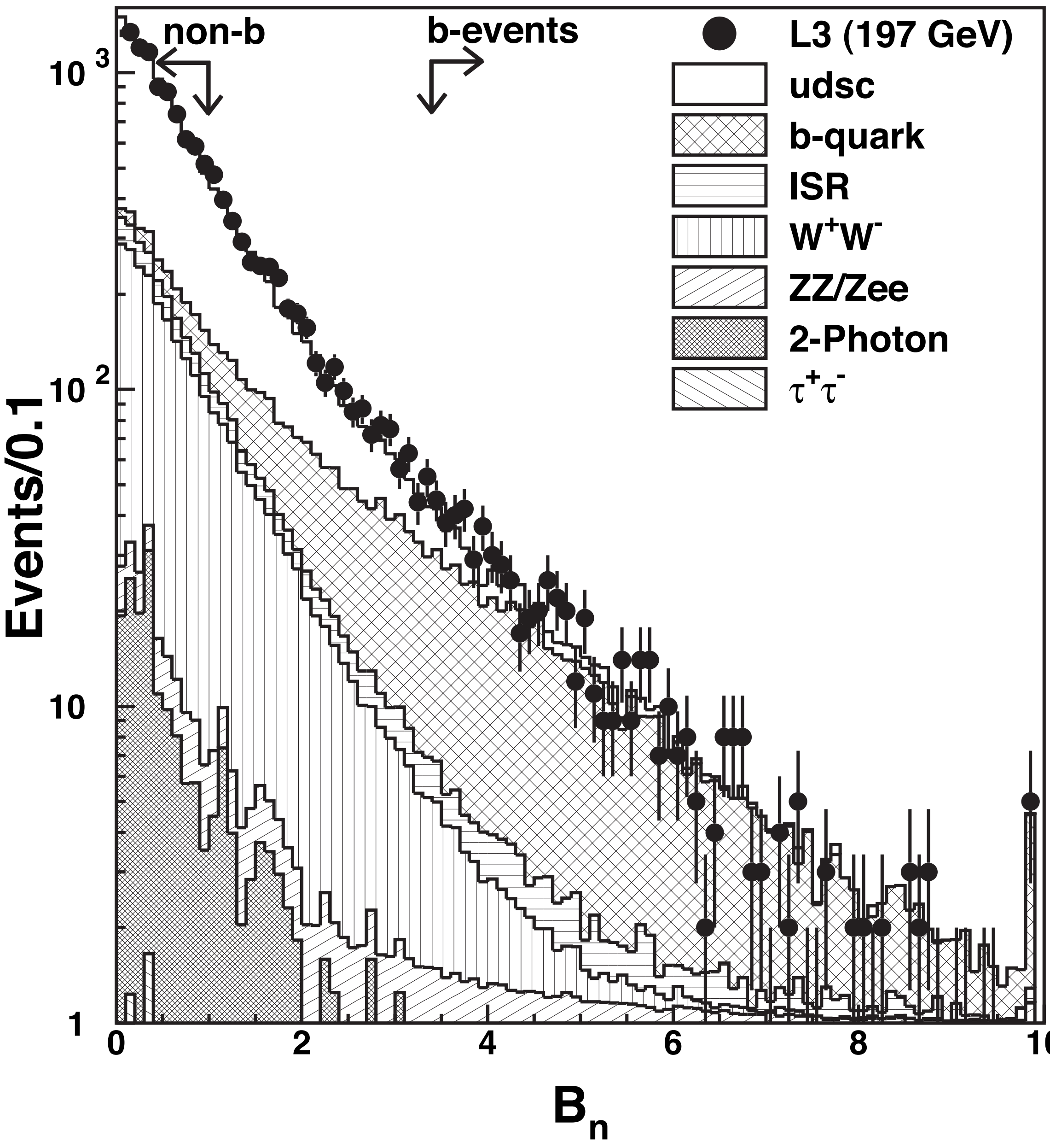

Figure 1: Distribution of the flavour tagging discriminator B_n for the combined data sample together with expectations from signal and background. The non-b events are selected using $B_\mathrm{n} < 1.0$. The b-events are selected with a cut on $B_\mathrm{n} > 3.4$.

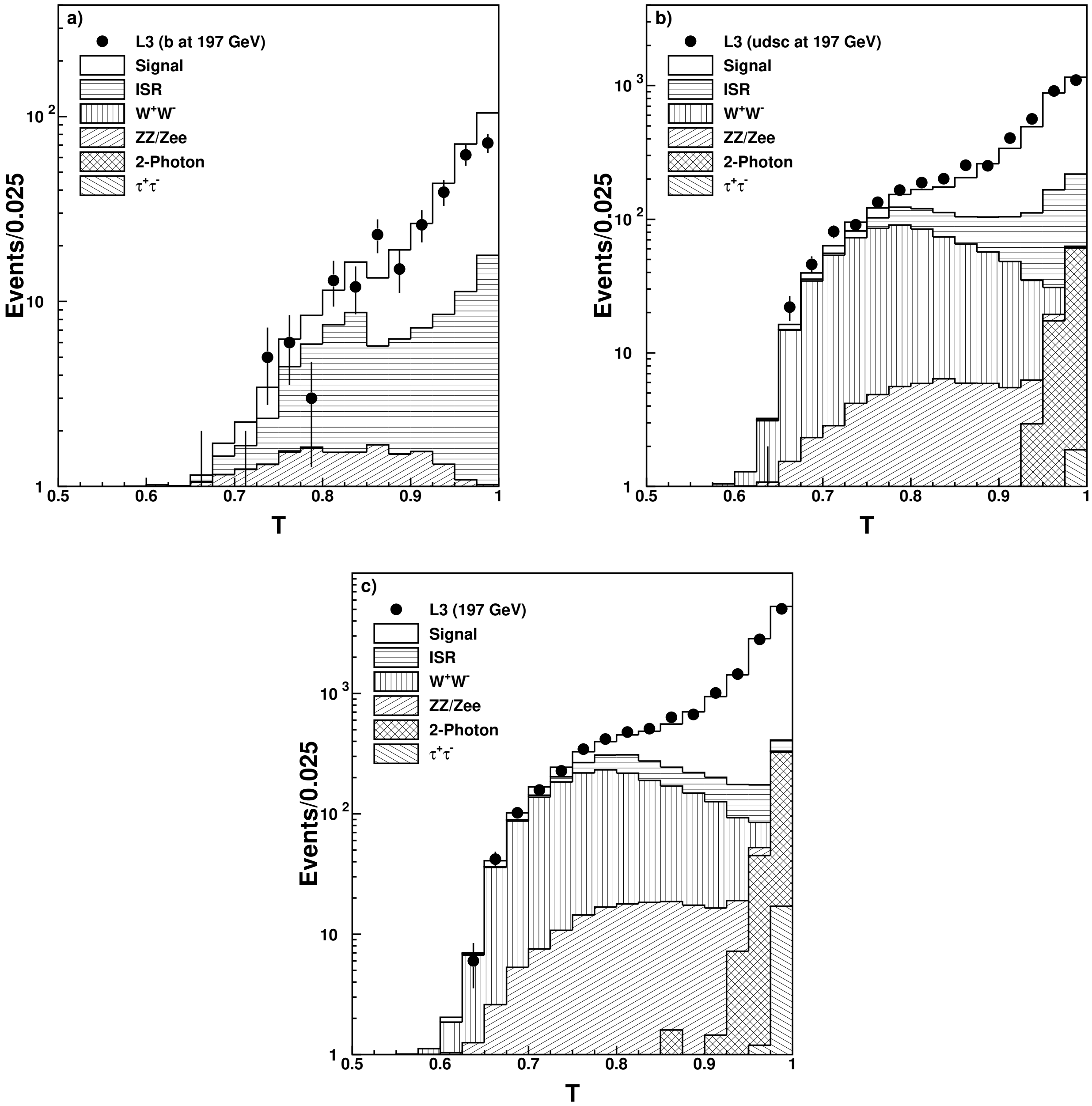

Figure 2: Thrust distribution at detector level at $\langle\sqrt{s}\rangle = 197$ GeV measured for (a) b-events (b) non-b events and (c) all events. The solid lines correspond to the overall expectation from theory. The shaded areas refer to different backgrounds and the white area refers to the signal as predicted by PYTHIA and KK2F.

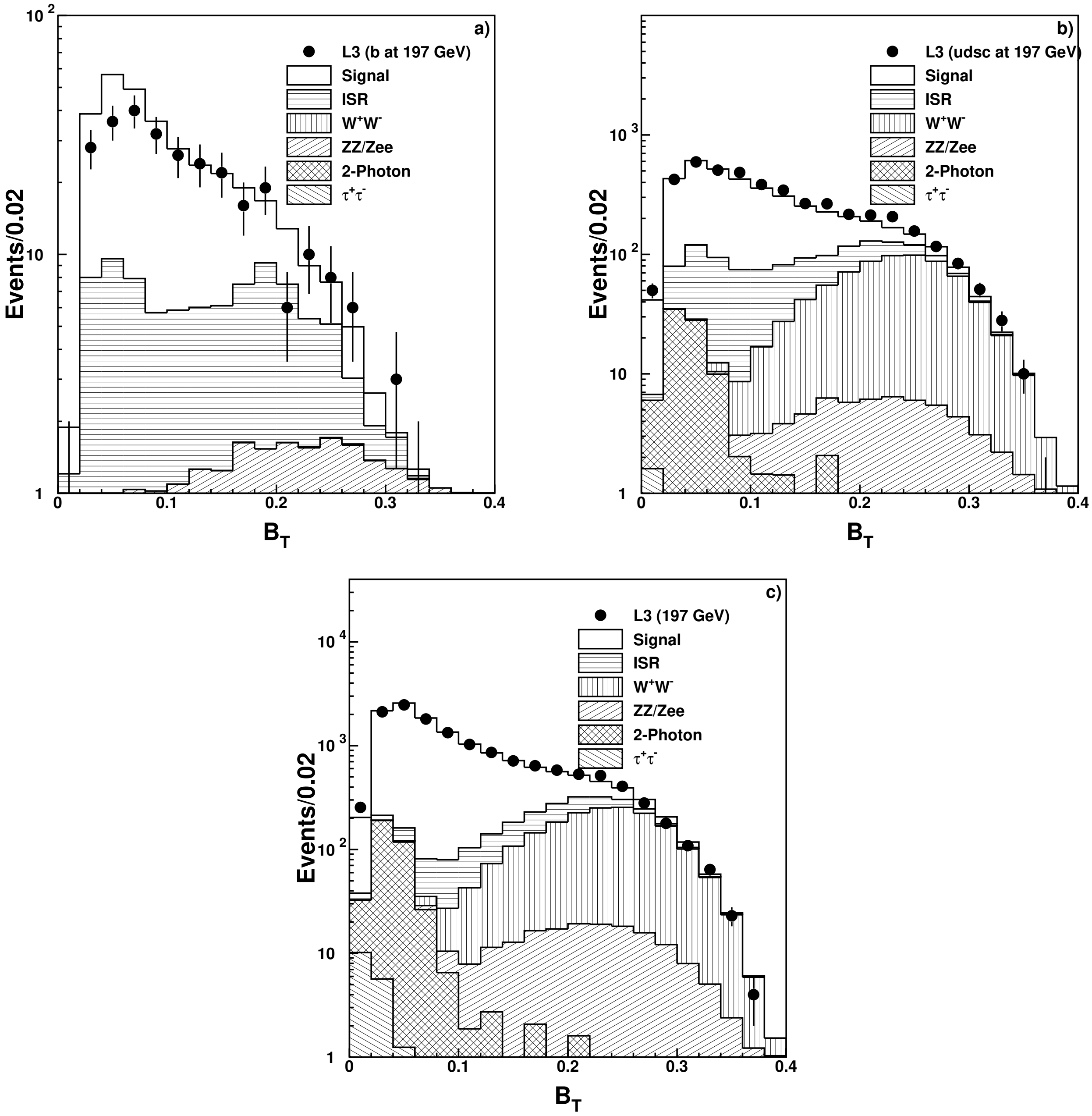

Figure 3: Measured total jet broadening distribution at $\langle\sqrt{s}\rangle = 197$ GeV for for (a) b-events (b) non-b events and (c) all events. The solid lines correspond to the overall expectation from theory. The shaded areas refer to different backgrounds and the white area refers to the signal as predicted by PYTHIA and KK2F.

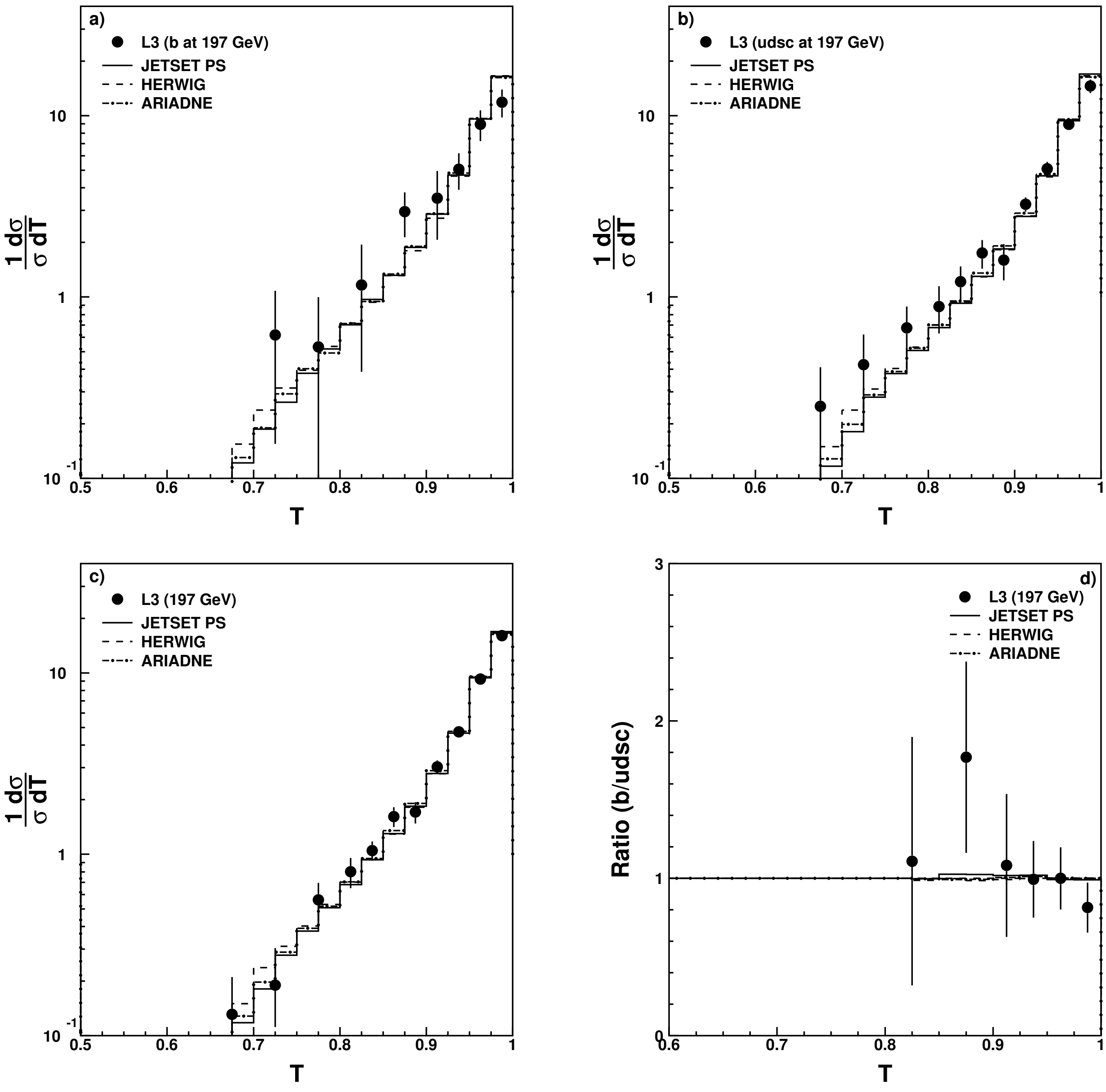

Figure 4: Thrust distributions at $\langle\sqrt{s}\rangle = 197$ GeV for a) b-events, b) non-b events, c) all events and d) the ratio between b- and non-b events compared to several QCD models.

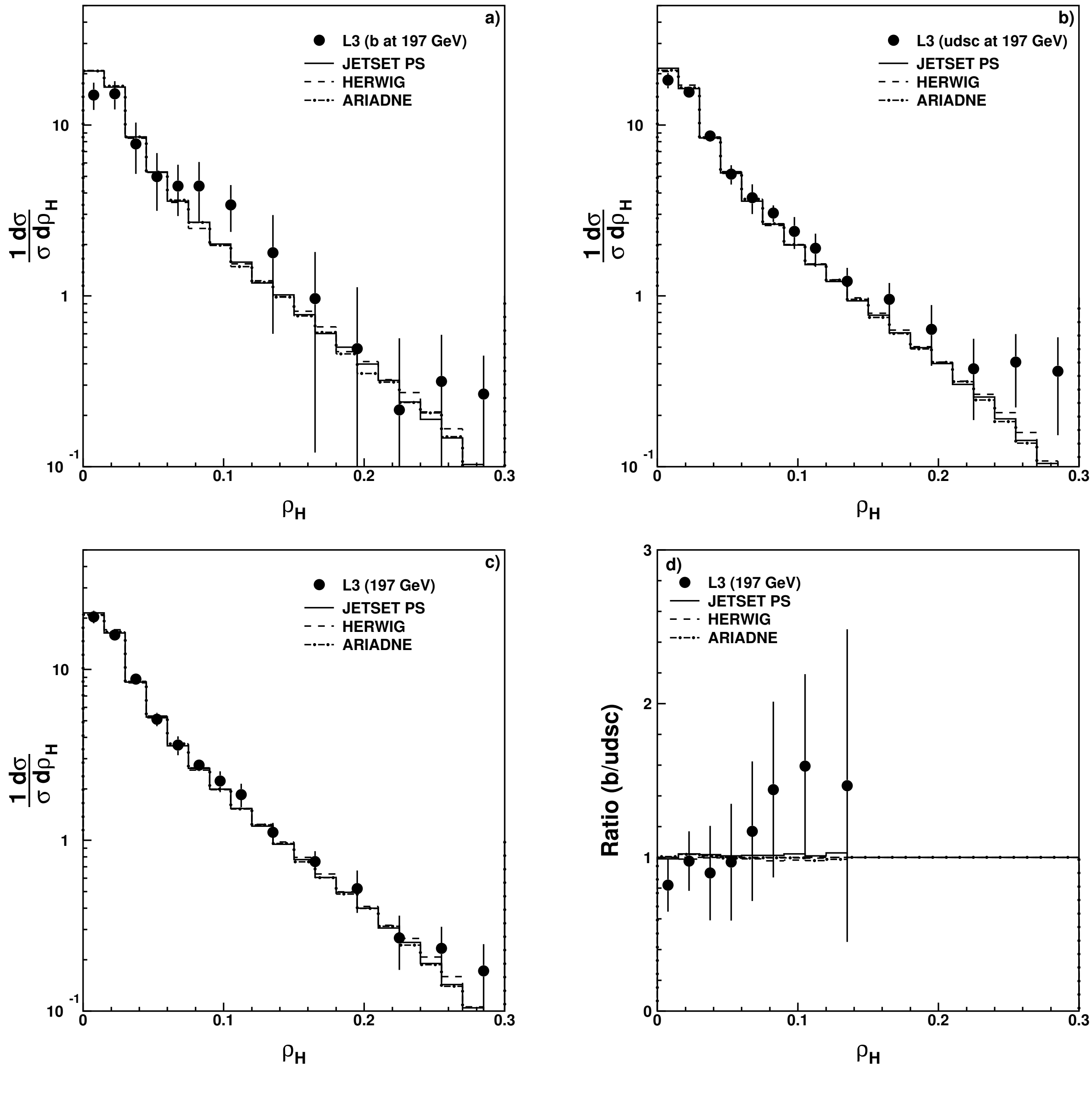

Figure 5: Scaled heavy jet mass distributions at $\langle\sqrt{s}\rangle$ = 197 GeV for a) b-events, b) non-b events, c) all events and d) the ratio between b- and non-b events compared to several QCD models.

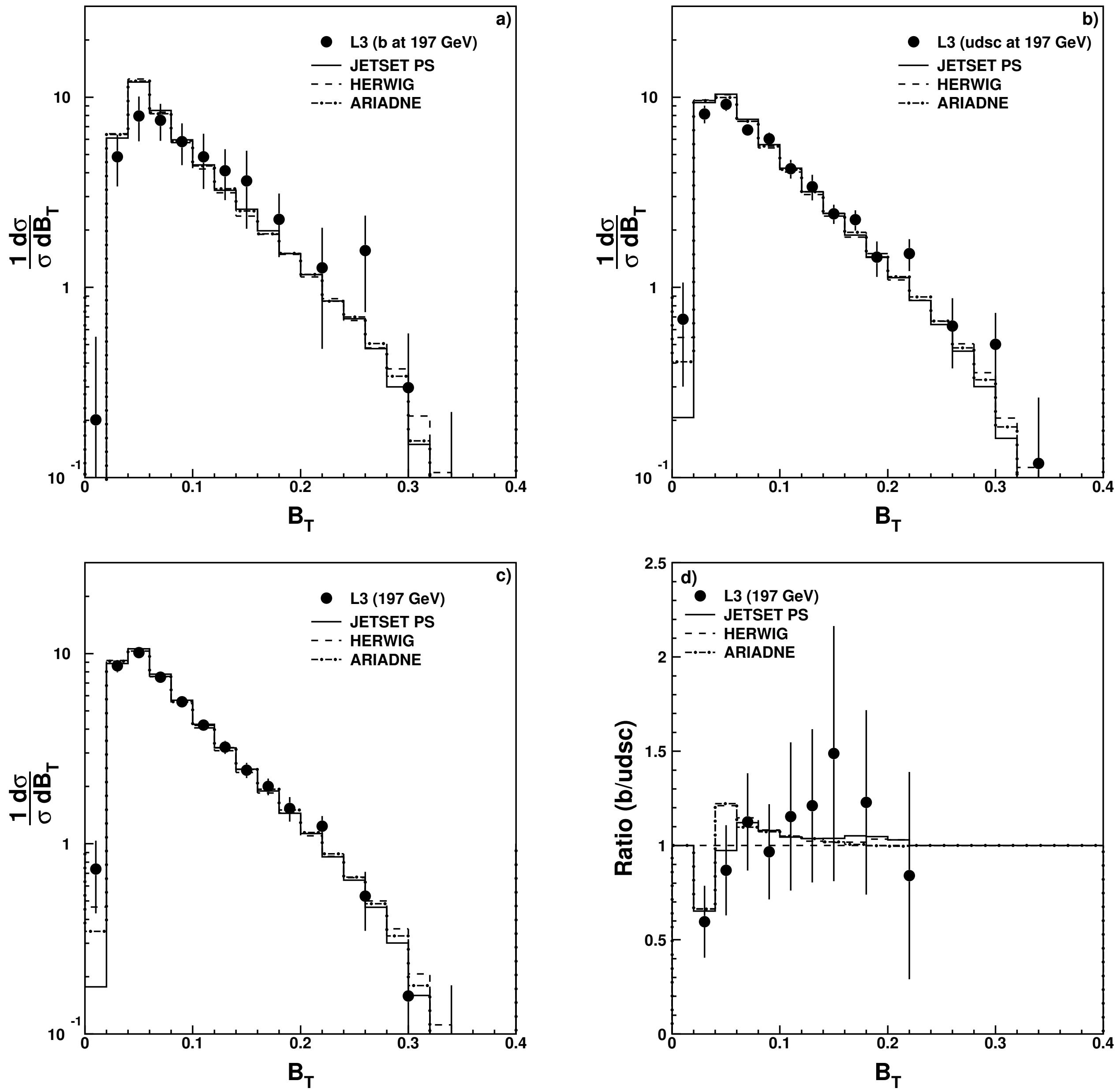

Figure 6: Total jet broadening distributions at $\langle\sqrt{s}\rangle = 197$ GeV for a) b-events, b) non-b events, c) all events and d) the ratio between b- and non-b events compared to several QCD models.

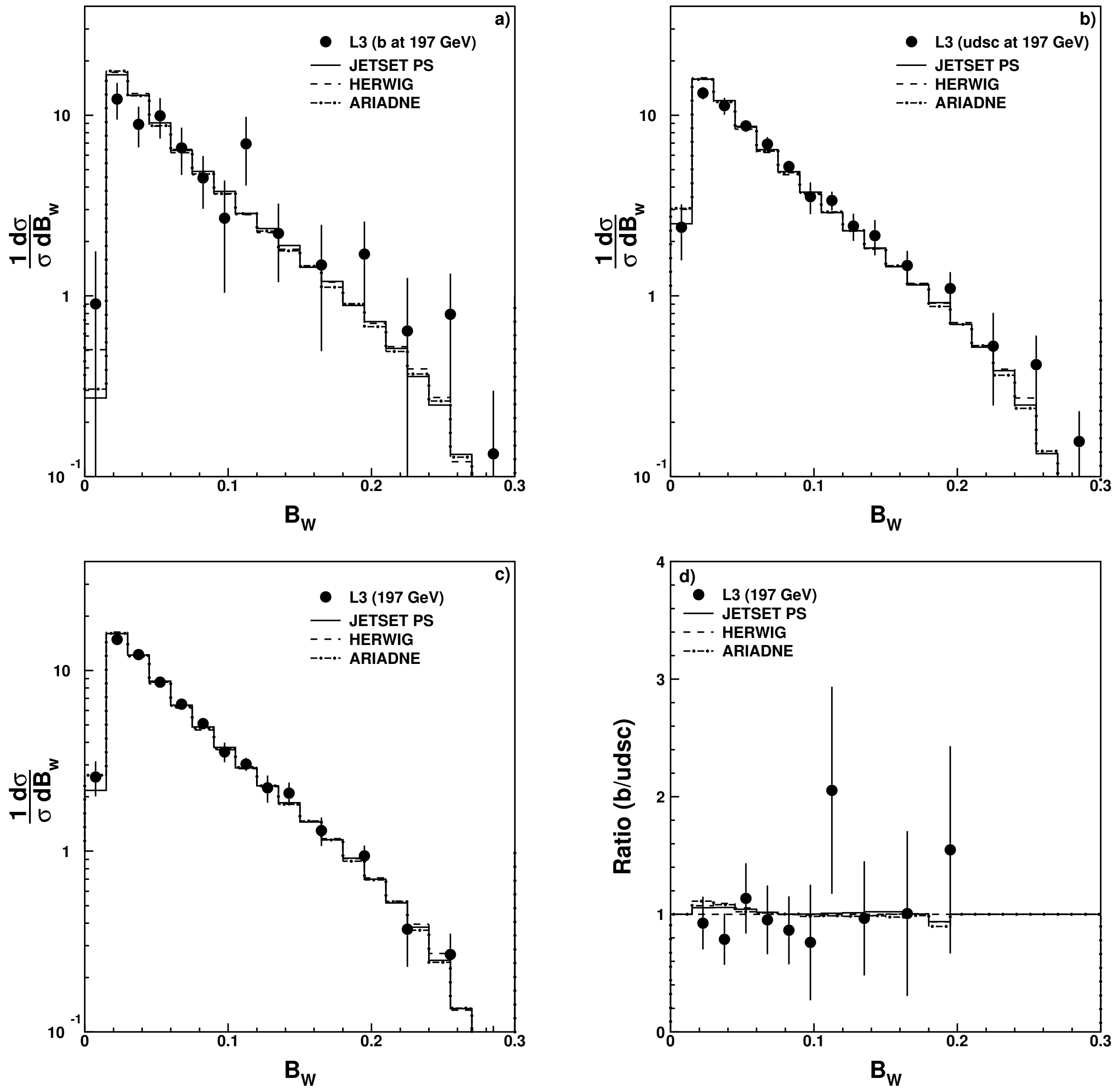

Figure 7: Wide jet broadening distributions at $\langle\sqrt{s}\rangle = 197$ GeV for a) b-events, b) non-b events, c) all events and d) the ratio between b- and non-b events compared to several QCD models.

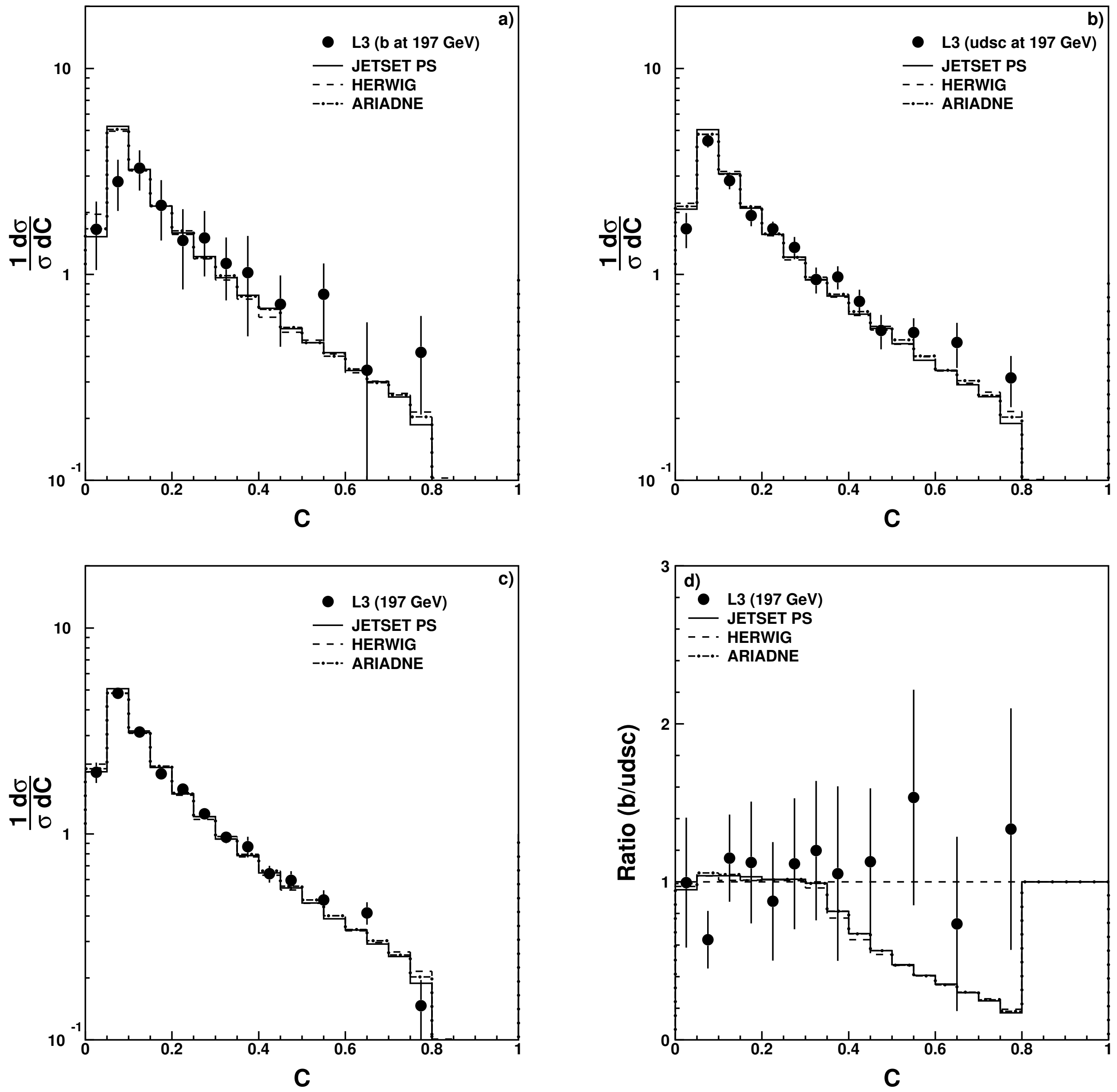

Figure 8: C-parameter distributions at $\langle\sqrt{s}\rangle = 197$ GeV for a) b-events, b) non-b events, c) all events and d) the ratio between b- and non-b events compared to several QCD models.

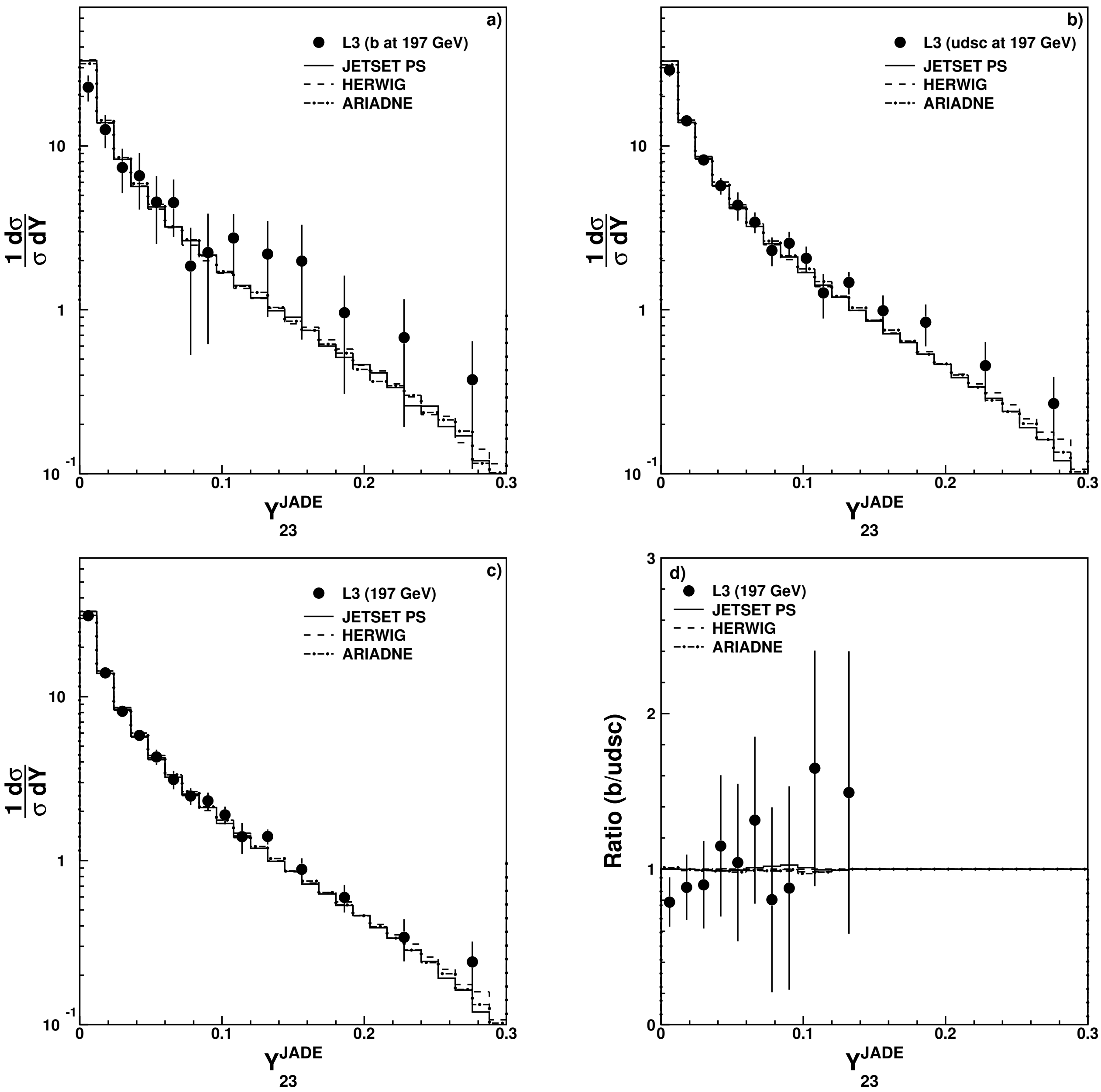

Figure 9: Jet resolution parameter (y_{23}^{J}) distributions for 2→3 jet in JADE algorithm at $\langle\sqrt{s}\rangle$ = 197 GeV for a) b-events, b) non-b events, c) all events and d) the ratio between b- and non-b events compared to several QCD models.